

# FedSKD: Aggregation-free Model-heterogeneous Federated Learning using Multi-dimensional Similarity Knowledge Distillation

Ziqiao Weng, Weidong Cai, Bo Zhou

**Abstract**—Federated learning (FL) enables privacy-preserving collaborative model training without direct data sharing. Model-heterogeneous FL (MHFL) extends this paradigm by allowing clients to train personalized models with heterogeneous architectures tailored to their computational resources and application-specific needs. However, existing MHFL methods predominantly rely on centralized aggregation, which introduces scalability and efficiency bottlenecks, or impose restrictions requiring partially identical model architectures across clients. While peer-to-peer (P2P) FL removes server dependence, it suffers from model drift and knowledge dilution, limiting its effectiveness in heterogeneous settings. To address these challenges, we propose FedSKD, a novel MHFL framework that facilitates direct knowledge exchange through round-robin model circulation, eliminating the need for centralized aggregation while allowing fully heterogeneous model architectures across clients. FedSKD’s key innovation lies in multi-dimensional similarity knowledge distillation, which enables bidirectional cross-client knowledge transfer at batch, pixel/voxel, and region levels for heterogeneous models in FL. This approach mitigates catastrophic forgetting and model drift through progressive reinforcement and distribution alignment while preserving model heterogeneity. Extensive evaluations on fMRI-based autism spectrum disorder diagnosis and skin lesion classification demonstrate that FedSKD outperforms state-of-the-art heterogeneous and homogeneous FL baselines, achieving superior personalization (client-specific accuracy) and generalization (cross-institutional adaptability). These findings underscore FedSKD’s potential as a scalable and robust solution for real-world medical federated learning applications.

**Index Terms**—Heterogeneous Model Federated Learning, Knowledge Distillation, Data Privacy, Feature Alignment, Classification.

## I. INTRODUCTION

ARTIFICIAL intelligence (AI)-based medical image analysis faces two fundamental challenges: the scarcity of annotated data and stringent privacy constraints. Unlike natural images, medical imaging data require specialized acquisition protocols, expensive equipment, and labor-intensive expert annotations [1]. These limitations reduce the availability of large-scale labeled datasets, impeding the development of robust deep learning (DL) models in this domain. While multi-institutional data sharing could alleviate this issue [2], strict privacy regulations, such as HIPAA [3], GDPR [4], and Cyber Security Law [5], make centralized data aggregation highly challenging in real-world scenarios.

Federated learning (FL) offers a promising solution by enabling collaborative model training without direct data

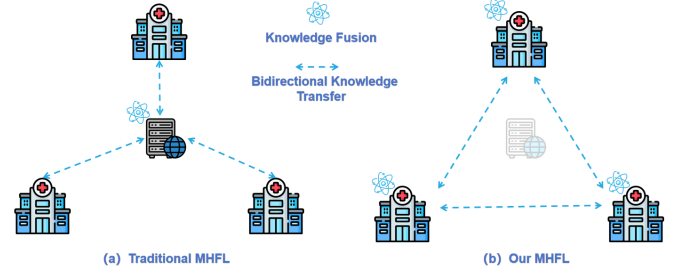


Fig. 1. Comparison of traditional MHFL schemes (a) and our proposed MHFL framework (b). Traditional MHFL methods rely on a central server for knowledge fusion and require partially identical model structures across clients. In contrast, our MHFL framework operates without a central server and allows fully heterogeneous model architectures while enabling direct knowledge transfer among clients.

sharing [1], [6], [7]. FL can be broadly categorized into central server-based and peer-to-peer approaches. In central server-based FL, institutions retain their data locally while iteratively training a shared global model, with a centralized server orchestrating the process. The widely used FedAvg algorithm [8] aggregates client model weights and distributes an updated global model in an iterative fashion. However, this approach often struggles with non-independent and identically distributions (non-IID) data distributions, which are prevalent in medical imaging due to variations, such as acquisition protocols, scanner types, and patient demographics [9], [10]. Naive weight averaging, as in FedAvg, can hinder model convergence and generalization [2], [11]. Several adaptations, such as FedProx [12], which introduces proximal regularization to stabilize local updates, and FedBN [13], which applies client-specific batch normalization layers, have been proposed to address this challenge. Additionally, domain adaptation [1], [14], [15] and knowledge distillation [11], [16]–[18] have been explored to mitigate the impact of data heterogeneity. On the other hand, peer-to-peer federated learning (P2P FL) [19]–[21] provides a decentralized alternative to server-based frameworks by facilitating direct model exchange among clients. This architecture inherently addresses non-IID data challenges through localized model refinement, eliminating the dependency on centralized aggregation. However, traditional decentralized aggregation methods [22]–[25] are constrained by three major limitations: excessive communication overhead, computational redundancy, and potential privacy risks arising from neighbor interactions. While recent advancements ([26], [27]) have proposed solutions to balance efficiency and privacy in data-heterogeneous FL, the biggest challenge is the lack of robust convergence and performance guarantees.

Z. Weng is with the Department of Radiology, Northwestern University, Chicago, IL, USA, and the School of Computer Science, The University of Sydney, Sydney, Australia. W. Cai is with the School of Computer Science, The University of Sydney, Sydney, Australia. B. Zhou is with the Department of Radiology, Northwestern University, Chicago, IL, USA. Corresponding email: bo.zhou@northwestern.edu

While data heterogeneity has been widely studied in FL, model heterogeneity remains a critical yet underexplored challenge. Variations in clients' computational resources and application-specific requirements often necessitate the use of heterogeneous model architectures [28]–[30]. Existing model-heterogeneous FL (MHFL) methods rely heavily on centralized aggregation and can be divided into two main approaches. The first, representation aggregation-dependent MHFL [28], [31]–[36], leverages a shared public dataset to facilitate knowledge distillation. However, obtaining such a dataset in privacy-sensitive medical domains is often impractical. The second approach, weight aggregation-dependent MHFL [37]–[43], aggregates partial or full model weights to align heterogeneous architectures. A common strategy involves co-training client-specific models alongside lightweight homogeneous counterparts, aggregating only the latter. However, persistent gradient conflicts caused by non-IID data can degrade convergence and generalization [27]. Moreover, this approach does not achieve full model heterogeneity, as part of the network architecture must remain consistent across clients. Additionally, both approaches rely on a central server, imposing high computational and storage demands that hinder scalability and communication efficiency. In contrast, P2P FL allows for direct training on diverse client architectures without the need for centralized aggregation.

However, P2P FL faces two significant challenges, as illustrated in Figure 2 (a): model drift and knowledge dilution. Model drift arises due to sequential fine-tuning across clients with heterogeneous data distributions, leading to unstable and inconsistent model performance. As models circulate through the network, essential features learned by early clients are progressively overwritten by subsequent local updates, resulting in catastrophic forgetting. Furthermore, existing P2P FL frameworks, whether based on parameter aggregation or alternative synchronization mechanisms, universally assume model homogeneity across clients. This assumption limits the flexibility of P2P frameworks in model-heterogeneous scenarios, where clients often use customized architectures tailored to their specific needs.

To address these issues, we propose FedSKD, a novel model-heterogeneous P2P FL framework based on multi-dimensional similarity knowledge distillation (SKD). FedSKD introduces two key innovations. First, it enables decentralized knowledge transfer by circulating locally trained heterogeneous models among clients in a round-robin manner, eliminating the gradient conflicts and server overhead inherent in traditional MHFL methods, as shown in Figure 1. In each training round, each client receives a model from the previous client, performs bidirectional knowledge distillation, and passes its enhanced model to the next client. This closed-loop knowledge reinforcement chain ensures that critical features are progressively amplified, rather than diluted, counteracting the problem of knowledge dilution. Second, FedSKD incorporates multi-dimensional similarity knowledge distillation to facilitate efficient cross-client knowledge reinforcement among heterogeneous models. Specifically, we introduce three novel SKD mechanisms that operate purely at the feature representation level: Batch-wise SKD (B-SKD) to align activation pat-

terns across batches, Pixel/Voxel-wise SKD (P-SKD) to align spatial feature distributions, and Region-wise SKD (R-SKD) to align representations within anatomical regions. During training, clients simultaneously distill domain-specific knowledge into received models while absorbing cross-institutional insights from these models, creating a bidirectional knowledge exchange that facilitates knowledge reinforcement and prevents model drift through continuous distribution alignment. We evaluate FedSKD on two clinically significant medical imaging tasks: fMRI-based autism spectrum disorder (ASD) diagnosis and skin lesion classification. Experimental results demonstrate that FedSKD outperforms existing methods in both personalization (client-specific performance) and generalization (cross-institutional adaptability), while addressing the challenges outlined above. These findings highlight FedSKD's potential to significantly advance federated learning in resource-constrained, need-variant, privacy-sensitive medical applications.

## II. METHOD

### A. Problem Definition

In this study, we investigate MHFL for supervised classification tasks in medical imaging. MHFL involves  $N$  clients where each FL client  $i$  possesses a local labeled dataset  $D_i$  and a unique local model  $M_i$ , defined by a specific architecture  $M_i$  and parameters  $\theta_i$ . Unlike traditional approaches, the local models can be heterogeneous across clients, such that  $M_i \neq M_j, i, j \in \{1, \dots, N\}$  for different clients  $i$  and  $j$ . All clients are assumed to perform the same classification task using data of the same modality. However, in real-world medical scenarios, the data distribution  $P_i$  of each client's dataset  $D_i$  is typically non-IID. This creates dual challenges: managing both model heterogeneity and data heterogeneity, which makes MHFL significantly more complex than conventional model-homogeneous federated learning. The goal of MHFL is to minimize the aggregated loss across all clients' heterogeneous local models with:

$$\min_{\theta_1, \dots, \theta_N} \sum_{i=1}^N \mathcal{L}(M_i(D_i)). \quad (1)$$

Our objective in this work is to train robust heterogeneous local models for each client through collaborative learning among decentralized clients without data sharing.

### B. Overall Framework of FedSKD

Figure 2 (b) provides an overview of the training process for our FedSKD framework, illustrating the steps followed during each communication round of the training:

① **Cross-Client Model Transfer Path Generation:** First, we determine a random route for transferring each client's local model across clients. In each training round, every client receives a model transferred from a randomly assigned, non-repeating client, ensuring a one-to-one mapping between models and clients. We define the order of the  $t$ th round as  $\mathcal{O}^t = \{\mathcal{O}_1^t, \dots, \mathcal{O}_N^t\} = \pi([1, 2, \dots, N])$ , where  $\pi(\cdot)$  represents the random permutation operation and  $\mathcal{O}_i^t$  represents the client index from which client  $i$  receives the cross-client model.

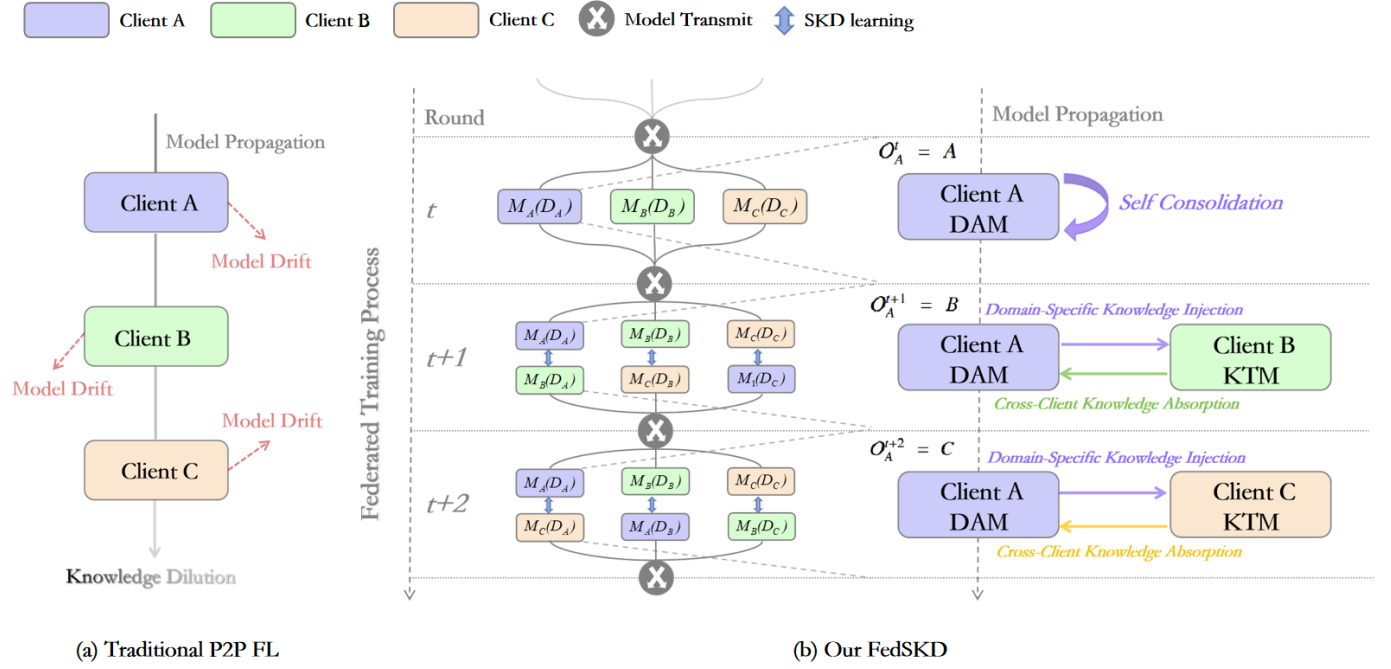


Fig. 2. (a) Traditional P2P FL methods are prone to model drift and knowledge dilution, limiting their effectiveness in MHFL. (b) Our FedSKD framework enhances knowledge transfer by circulating heterogeneous models among clients in a round-robin manner guided by a predefined order  $\mathcal{O}$ . During non-transfer phases, clients refine their personalized domain-adaptive models (DAM) locally. In transfer phases, bidirectional knowledge transfer occurs between the local DAM and the received knowledge-transit model (KTM) through multi-dimensional similarity knowledge distillation (SKD). This process allows the DAM to share domain-specific knowledge with the KTM, while the KTM provides cross-client insights to the DAM, ensuring continuous knowledge reinforcement and mitigating model drift through consistent distribution alignment.

In this framework, we refer to the client's local model as the **Domain-Adaptive Model (DAM)**, which specializes in adapting to the local data distribution, and the received model as the **Knowledge-Transit Model (KTM)**, which serves as a carrier of cross-client knowledge. This structured method ensures efficient and unbiased knowledge propagation while maintaining the individuality of each client's model.

② **Bidirectional Knowledge Distillation:** At the beginning of each round, each client receives a copy of a latest model transmitted from its assigned remote client according to  $\mathcal{O}^t$ . Taking client  $i$  as an example, if  $\mathcal{O}_i^t = i$ , the client  $i$  performs self consolidation, locally refining its DAM solely on  $D_i$  through standard supervised learning. Conversely, if  $\mathcal{O}_i^t = j$ , ( $i \neq j$ ), client  $i$  performs bidirectional knowledge distillation between its local DAM  $M_i$  and the received KTM  $\tilde{M}_j$ .

The distillation progresses through two concurrent knowledge flows: **Domain-Specific Knowledge Injection (DAM  $\rightarrow$  KTM)**: client  $i$ 's DAM  $M_i$  acts as a local expert, distilling its domain-specific expertise from  $D_i$  into the received KTM  $\tilde{M}_j$  through multi-dimensional SKD. **Cross-Client Knowledge Absorption (KTM  $\rightarrow$  DAM)**: Simultaneously, The client  $j$ 's KTM  $\tilde{M}_j$  serves as a carrier of cross-client knowledge, providing complementary insights to enhance the generalization capability of the client  $i$ 's DAM  $M_i$ . In addition to mutual distillation, client  $i$ 's DAM  $M_i$  receives direct supervision from  $D_j$  to facilitate local adaptation and client  $j$ 's KTM  $\tilde{M}_j$  continues local training on  $D_j$  to maintain base performance and avoid severe model drift. This dual-phase process guarantees progressive knowledge refinement as received KTMs

adapt to local distributions while retaining cross-client knowledge, and local DAMs assimilate refined knowledge through reciprocal distillation. Catastrophic forgetting (i.e. knowledge dilution) is mitigated via multi-dimensional SKD's feature-space regularization (detailed in Section II-C).

③ **Model Decomposition and Knowledge Preservation:** We decompose the model into two functionally distinct components: a feature extractor, which transforms raw input data into high-level feature representations, and a prediction header, which serves as a classifier to generate final predictions based on these features. Our primary objective is to ensure that, during adaptation to the target data distribution, the received model retains its previously acquired cross-client knowledge, rather than allowing the target domain's knowledge to progressively overwrite it. To achieve this, we freeze the parameters of the received model's prediction header and only finetuning the feature extractor during mutual learning. This constraint serves two critical purposes: 1) it prevents the feature extractor from over-adapting to the target domain, thereby preserving the cross-client knowledge embedded in the model, and 2) it regularizes the shift in feature representations from the received model's domain to the target domain, ensuring stable and generalizable feature alignment.

④ **Model Update and Propagation:** Upon completing the training in the  $t$ -th round, each client discards the received model (KTM) and retains only its updated and enhanced local model (DAM). The updated models are then propagated to new clients in the subsequent round according to the permutation order  $\mathcal{O}^{t+1}$ , ensuring continuous and structured knowledge

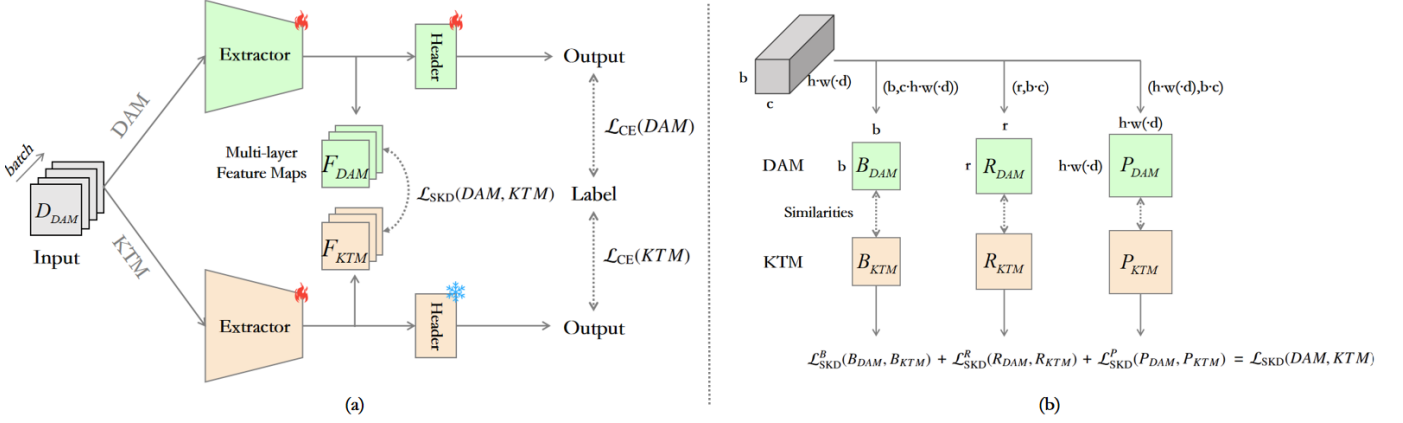


Fig. 3. (a) Overview of the FedSKD training framework: Multi-dimensional similarity knowledge distillation facilitates the mutual distillation of semantically meaningful knowledge between the local DAM and the received KTM (Figure 2). Both models are jointly optimized on the DAM's dataset, leveraging supervised learning with corresponding dataset labels. The snowflake icon signifies frozen parameters, whereas the flame icon represents active parameter updates during training. (b) Computation of multi-dimensional similarity knowledge distillation loss: The loss is calculated by measuring divergence between the learned similarity patterns of the DAM and KTM across multiple granularities (Batch-wise, Pixel/Voxel-wise, Region-wise), ensuring effective knowledge transfer and alignment.

exchange across the network. This iterative process enables progressive model refinement while maintaining decentralized coordination.

⑤ **Joint Optimization Objective:** The total loss of SKD training at the  $t$ -th stage on a client can be defined as follows:

$$\begin{aligned} \mathcal{L}(M_i^t, \tilde{M}_j^t) = & \mathcal{L}_{CE}(M_i^t(x_i), y_i) \\ & + \gamma \cdot \mathcal{L}_{SKD}(M_i^t(x_i), \tilde{M}_j^t(x_i)) \\ & + \mathcal{L}_{CE}(\tilde{M}_j^t(x_i), y_i) \end{aligned} \quad (2)$$

where  $\mathcal{L}_{CE}$  and  $\mathcal{L}_{SKD}$  denotes the cross-entropy loss and our multi-dimensional similarity knowledge distillation loss (to be elaborated in Section II-C). Here,  $\gamma$  is a balancing hyperparameter, and  $(x_i, y_i) \sim D_i$ .

The global optimization objective during this stage thus can be formulated as:

$$\min_{\theta_1, \dots, \theta_N} \sum_{i=1}^N \mathcal{L}(M_i^t, \tilde{M}_{O^t}^t). \quad (3)$$

The above steps are iteratively performed until the local models of all clients have converged across the entire set of client datasets. Subsequently, each client retains its respective model for the purposes of federated learning deployment and inference.

### C. Multi-dimensional Similarity Knowledge Distillation

We propose a multi-dimensional similarity knowledge distillation approach within the context of our model-heterogeneous federated learning (FL) framework (Figure 3). The specifics of this approach are detailed below:

**Notation:** Without loss of generality, we consider a 2D scenario here. Given a mini-batch input, denote the feature map produced by the local model  $DAM$  at a particular layer  $\ell$  by  $F_{DAM}^\ell \in \mathbb{R}^{b \times c \times h \times w}$ , and the feature map produced by the received network  $KTM$  at a particular layer  $\ell'$  by

$F_{KTM}^{\ell'} \in \mathbb{R}^{b \times c' \times h' \times w'}$ , where  $b$  is the batch size,  $c$  is the channel number, and  $h$  and  $w$  are spatial dimensions. Note that  $c', h', w'$  do not necessarily have to be identical to  $c, h, w$ , as the models are heterogeneous. In our setting, since the local network and the received network have the same depth (i.e., the number of blocks), we let  $\ell = \ell'$ , meaning that we perform knowledge distillation at the same layer for both the local model  $DAM$  and the received model  $KTM$ . We denote  $\mathbb{L}$  as the set of all  $\ell$  in knowledge distillation process.

**Batch-wise Similarity** quantifies inter-sample semantic relationships across categories within a mini-batch. The batch-wise similarity loss guides the local model  $DAM$  and the received model  $KTM$  towards capturing identical dataset-specific semantic patterns. We first reshape the feature map  $F_{DAM}^\ell$  of the DAM to  $H_{DAM}^\ell \in \mathbb{R}^{b \times chw}$ . We then compute the batch-wise similarity induced in the DAM's feature map  $F_{DAM}^\ell$  as follows:

$$B_{DAM}^\ell = \frac{H_{DAM}^\ell \cdot (H_{DAM}^\ell)^T}{\|H_{DAM}^\ell \cdot (H_{DAM}^\ell)^T\|_2^{(1)}} \cdot \sqrt{b} \quad (4)$$

where  $B_{DAM}^\ell$  is a  $b \times b$  matrix, and  $\|\cdot\|_2^{(1)}$  is the row-wise L2 normalization (i.e. in  $\text{dim}=1$  of the matrix). Each item in the matrix is indirectly divided by  $\sqrt{b}$  during the computation, so we multiply by  $\sqrt{b}$  at the end to scale the values back, bringing them to the same magnitude as other forms of similarity. Intuitively, the entry  $(i, j)$  in  $B_{DAM}^\ell$  represents the scaled similarity activated at layer  $\ell$  of the DAM between the  $i$ -th and  $j$ -th images in the mini-batch. Analogously, the batch-wise similarity in the KTM can be calculated by:

$$B_{KTM}^\ell = \frac{H_{KTM}^\ell \cdot (H_{KTM}^\ell)^T}{\|H_{KTM}^\ell \cdot (H_{KTM}^\ell)^T\|_2^{(1)}} \cdot \sqrt{b} \quad (5)$$

Then, we define the batch-wise similarity knowledge distil-

lation loss as:

$$\mathcal{L}_{\text{SKD}}^B(B_{DAM}, B_{KTM}) = \frac{1}{|\mathbb{L}|} \sum_{\ell \in \mathbb{L}} \frac{1}{b^2} \|B_{DAM}^\ell - B_{KTM}^\ell\|_F^2 \quad (6)$$

**Pixel/Voxel-wise Similarity** measures fine-grained semantic correspondences at individual spatial units (pixels/voxels). The pixel/voxel-wise similarity loss enforces spatial consistency between the feature representations of the *DAM* and the *KTM*, ensuring that both models align in their understanding of local structural patterns and spatial relationships within a mini-batch. We first reshape the feature map  $F_{DAM}^\ell$  of the *DAM* to  $H_{DAM}^\ell \in \mathbb{R}^{hw \times bc}$ . We then compute the pixel-wise similarity induced in the *DAM*'s feature map  $F_{DAM}^\ell$  as follows:

$$P_{DAM}^\ell = \frac{H_{DAM}^\ell \cdot (H_{DAM}^\ell)^T}{\|H_{DAM}^\ell \cdot (H_{DAM}^\ell)^T\|_2^{(1)}} \cdot \sqrt{hw} \quad (7)$$

Analogously, the pixel-wise similarity in the *KTM* can be calculated by:

$$P_{KTM}^\ell = \frac{H_{KTM}^\ell \cdot (H_{KTM}^\ell)^T}{\|H_{KTM}^\ell \cdot (H_{KTM}^\ell)^T\|_2^{(1)}} \cdot \sqrt{hw} \quad (8)$$

Then, we can define the pixel-wise similarity knowledge distillation loss as:

$$\mathcal{L}_{\text{SKD}}^P(P_{DAM}, P_{KTM}) = \frac{1}{|\mathbb{L}|} \sum_{\ell \in \mathbb{L}} \frac{1}{hw^2} \|P_{DAM}^\ell - P_{KTM}^\ell\|_F^2 \quad (9)$$

Given the potential structural heterogeneity of models, it is necessary to align  $P_{DAM}$  and  $P_{KTM}$  to the same spatial dimension before computing the loss, especially when their spatial dimensions are mismatched. This dimension-matching step can be straightforwardly achieved using various spatial interpolation techniques, such as bilinear interpolation.

**Region-wise Similarity** captures semantic correlations between meaningful, interrelated regions within a given modality. The region-wise similarity loss enforces consistency between the *DAM* and the *KTM*, guiding both models to learn similar inter-region correlations within a mini-batch. For instance, in neuroimaging, the brain is partitioned into functional regions, which exhibit strong interdependencies despite anatomical separation [44], [45]. Such region-based correlations are crucial for understanding complex systems, making region-wise similarity a powerful tool for capturing high-level relationships in diverse applications. Given an image with  $r$  predefined regions, let  $M_k$  be the collection of all pixels  $(i, j)$  belonging to the  $k$ th region. We first compute the feature corresponding to the  $k$ th region by averaging the features within this region as follows:

$$H_k^{(b,c)} = \frac{1}{|M_k|} \sum_{(i,j) \in M_k} F^{(b,c,h,w)}(i, j) \quad (10)$$

Then, we can get the region-wise feature maps via:

$$H^{(b,r,c)} = [H_1^{(b,c)}, H_2^{(b,c)}, \dots, H_r^{(b,c)}], \quad (11)$$

where the output can then be reshaped as  $H \in \mathbb{R}^{r \times bc}$ . Similarly, we compute the region-wise similarity induced in

the *DAM*'s feature map  $F_{DAM}^\ell$  and the *KTM*'s feature map  $F_{KTM}^\ell$  as follows:

$$R_{DAM}^\ell = \frac{H_{DAM}^\ell \cdot (H_{DAM}^\ell)^T}{\|H_{DAM}^\ell \cdot (H_{DAM}^\ell)^T\|_2^{(1)}} \cdot \sqrt{r}, \quad (12)$$

$$R_{KTM}^\ell = \frac{H_{KTM}^\ell \cdot (H_{KTM}^\ell)^T}{\|H_{KTM}^\ell \cdot (H_{KTM}^\ell)^T\|_2^{(1)}} \cdot \sqrt{r}. \quad (13)$$

Given above, we define the region-wise similarity knowledge distillation loss as:

$$\mathcal{L}_{\text{SKD}}^R(R_{DAM}, R_{KTM}) = \frac{1}{|\mathbb{L}|} \sum_{\ell \in \mathbb{L}} \frac{1}{r^2} \|R_{DAM}^\ell - R_{KTM}^\ell\|_F^2 \quad (14)$$

Combining all above, we then define the total loss of multi-dimensional similarity knowledge distillation as:

$$\begin{aligned} \mathcal{L}_{\text{SKD}}(DAM, KTM) &= \mathcal{L}_{\text{SKD}}^B(B_{DAM}, B_{KTM}) \\ &\quad + \mathcal{L}_{\text{SKD}}^P(P_{DAM}, P_{KTM}) \\ &\quad + \mathcal{L}_{\text{SKD}}^R(R_{DAM}, R_{KTM}) \end{aligned} \quad (15)$$

Please note that if the dataset does not have predefined region masks, the region-wise similarity loss is optional.

### III. EXPERIMENTS AND RESULTS

The experiments were conducted on two challenging classification tasks using real-world medical imaging datasets to assess the effectiveness of our methods. In the following sections, we detail our tasks and datasets (Section III-A), experimental setups (Section III-B), and experimental results (Section III-C).

#### A. Tasks and Datasets

##### 1) fMRI-based Autism Spectrum Disorder Classification:

**Task Description:** Autism Spectrum Disorder (ASD) is a neurodevelopmental disorder characterized by impairments in social interaction, communication, learning, and behavior [46]. Early diagnosis is crucial for enabling timely and effective interventions. Resting-state functional magnetic resonance imaging (rs-fMRI) has emerged as a widely used non-invasive tool for capturing brain connectivity patterns, making it a valuable resource for the early diagnosis of neurological disorders. In this study, we leverage rs-fMRI data to differentiate individuals with ASD from typical controls (TC), framing the problem as a binary classification task.

**Dataset Description:** We utilize the publicly available ABIDE-I dataset [47], which includes data from 1,112 subjects with 539 diagnosed with ASD and 573 healthy controls. The data is collected across 17 sites in North America and Europe, which encompasses T1-weighted structural brain images, fMRI scans, and detailed phenotypic information for each subject. Following rigorous quality control and the exclusion of incomplete or corrupted data, we retained a final dataset of 871 subjects (403 with ASD and 468 healthy controls). Preprocessing was performed using the Connectome Computation System (CCS) pipeline. Nuisance signal removal was



then applied to mitigate confounding variations arising from head motion, physiological processes (e.g., heartbeat and respiration), and scanner drift. After nuisance regression, a band-pass filter (0.01–10 Hz) was applied, excluding global signal correction. Spatial normalization was subsequently conducted to align the brain images with the Montreal Neurological Institute (MNI) template, achieving a standardized resolution of  $3 \times 3 \times 3 \text{ mm}^3$ . In this study, we adopt the methodology proposed in STO [48], utilizing 3D statistical derivatives that preserve the full spatial resolution  $61 \times 73 \times 61$  of the original 4D fMRI data as network input. These derivatives include Regional Homogeneity (ReHo), Degree Centrality (DC), Local Functional Connectivity Density (LFCd), and Voxel-Mirrored Homotopic Connectivity (VMHC). For further details on these derivatives, we refer readers to [49].

**Non-IID Dataset Construction:** The ABIDE dataset is aggregated from 17 distinct medical centers across geographically diverse regions, with each institution employing distinct assessment protocols and data acquisition procedures, including variations in MRI scanner specifications and imaging parameters. Consequently, the ABIDE dataset inherently exhibits a non-independent and non-identically distributed (non-IID) data structure. Prior methodologies for processing ABIDE data have employed two primary strategies: 1) selecting subsets of large medical sites as FL clients [1], [14], [50], or 2) centralized aggregation followed by random data partitioning across clients [6]. The first strategy neglects smaller contributing sites, whereas the second approach fails to preserve institutional heterogeneity due to potential inter-client data overlap from shared medical centers. To address these limitations, this paper proposes a geographically stratified non-IID partitioning strategy. The 17 sites are stratified into four geographically coherent regions: Europe, Western USA, Central USA, and Eastern USA (see Table I). This partitioning ensures that each FL client represents a unique geographic region, preserving data heterogeneity and minimizing inter-client overlap. The resulting dataset is referred to as FedASD.

TABLE I  
DISTRIBUTION OF NON-IID DATA ACROSS CLIENTS IN OUR FEDASD DATASET. FOUR GEOGRAPHICALLY DIFFERENT REGIONS ARE CLUSTERED AND DEFINED AS FOUR DIFFERENT CLIENTS.

Client	Site	Region	Diagnosis (ASD/TC)	Total (ASD/TC)
1 (Europe)	LEUVEN	Belgium	26/30	172 (76/96)
	MAX_MUN	Germany	19/27	
	TRINITY	Ireland	19/25	
	SBL	Netherlands	12/14	
2 (West USA)	UCLA	CA, USA	48/37	244 (128/116)
	USM	UT, USA	43/24	
	SDSU	CA, USA	8/19	
	STANFORD	CA, USA	12/13	
	OHSU	OR, USA	12/13	
	CALTECH	CA, USA	5/10	
3 (Middle USA)	UM	MI, USA	47/73	181 (77/104)
	PITT	PA, USA	24/26	
	CMU	PA, USA	6/5	
4 (East USA)	NYU	NY, USA	74/98	274 (122/152)
	YALE	CT, USA	22/19	
	KKI	MD, USA	12/21	
	OLIN	CT, USA	14/14	

2) *Skin Lesion Classification: Task Description:* Skin cancer, particularly melanoma, remains one of the most lethal malignancies. Early detection of melanoma not only can

significantly reduce treatment costs but can enhance patient survival [51], [52]. Dermoscopy is one of the most widely adopted non-invasive imaging techniques to capture detailed morphological and visual characteristics of pigmented lesions for this purpose [51]. In this study, we utilize dermoscopic images to diagnose skin lesions, framing the problem as a multi-class classification task.

**Dataset Description:** We utilized the publicly available Derm7pt dataset [51], which comprises dermoscopic images, clinical images, and associated meta-data. Dermoscopic images are obtained using a dermatoscope with a standardized field of view and controlled acquisition conditions. The patient meta-data encompasses additional details, such as gender and lesion location [51]. In Derm7pt, 20 distinct skin lesion conditions were categorized into five primary types: basal cell carcinoma (BCC), nevus (NEV), melanoma (MEL), miscellaneous (MISC), and seborrheic keratosis (SK). Lesions within each category share similar clinical interpretations. The Derm7pt dataset consists of 1,011 cases, with 42 BCC, 575 NEV, 252 MEL, 97 MISC, and 45 SK lesions. All images have been resized to  $512 \times 512 \times 3$  pixels. Our focus is on diagnosing the five types of skin lesions using dermoscopic images.

**Non-IID Dataset Construction:** The Skin dataset adheres to strict consistency in imaging acquisition protocols, with standardized scanner configurations and processing pipelines across all samples. To systematically model non-IID data distributions, we adopt a Dirichlet distribution ( $Dir(\alpha)$ ), a probabilistic framework that enables controlled simulation of data heterogeneity by perturbing the original IID structure. Specifically, for a dataset with  $C$  classes and  $N$  clients, we generate an  $N$ -dimensional probability vector  $p_c = \{p_{c,1}, \dots, p_{c,N}\} \sim Dir(\alpha)$  for each class  $c$ , where  $\sum_{i=1}^N p_{c,i} = 1$  and each element  $p_{c,i}$  represents the proportion of class  $c$  samples assigned to client  $i$ . By partitioning class instances across FL clients based on the concentration parameter  $\alpha$ , this approach allows for precise control over data distribution skewness. Lower values of  $\alpha$  induce a more pronounced skew, thereby accentuating non-IID characteristics. In our study, we construct three FL clients and implement two distinct non-IID scenarios using  $\alpha \in \{1.0, 0.5\}$ , as shown in Figure 4. This dual mechanism, encompassing both label and quantity skew, reflects real-world medical imaging constraints where class imbalances and uneven data collection practices are prevalent. The resulting dataset is designated as FedSkin.

## B. Experimental Setup

1) *Baselines:* We evaluate our method by conducting comprehensive comparisons against baselines from both model-homogeneous and model-heterogeneous FL scenarios, which include seven baselines. In the model-homogeneous FL setting, all clients are equipped with a ResNet-10 model featuring a fixed channel size of 64. In contrast, the model-heterogeneous FL setting employs the same ResNet-10 architecture across all clients but introduces variability in the initial channel sizes to simulate heterogeneity. Specifically, the first client is assigned a channel size of 64, the second

client 62, and each subsequent client’s channel size decreases by 2, thereby progressively increasing the degree of model heterogeneity. Baselines from both model-homogeneous and model-heterogeneous FL are summarized in the following:

**Centralized:** An ideal scenario where all clients’ data can be freely shared among clients without privacy constraints. Each client’s model is trained on the entire dataset assembled from all clients, serving as a theoretical upper-bound performance benchmark.

**Local:** In this setting, each client’s model is trained solely on its own private dataset, with no communication between clients. This approach more accurately reflects real-world medical applications, where data privacy and security are paramount considerations.

**FedAvg:** A foundational FL algorithm where clients train models locally and aggregate parameters through model averaging after each communication round. FedAvg is designed for model-homogeneous settings and often struggles with non-IID data distributions.

**FedProx:** An extension of FedAvg that introduces a proximal term to regulate local model updates, enhancing convergence stability in heterogeneous data or system environments. However, it remains infeasible to model-homogeneous settings.

**FedBN:** This method addresses feature shifts in non-IID data by preserving client-specific batch normalization (BN) layers while aggregating other parameters globally. While effective in heterogeneous data environments, FedBN is constrained to model-homogeneous architectures.

**FedCross:** This approach is considered the SOTA P2P FL approach that eliminates model aggregation by circulating a single global model among clients for sequential training. FedCross is designed for model-homogeneous settings and does not support architectural heterogeneity.

**FedCross<sup>†</sup>** While FedCross was developed for homogeneous-model FL setting, its P2P characteristics allow its natural extension to heterogeneous-model FL setting. Thus, we adapted a variant of FedCross here (i.e. FedCross<sup>†</sup>) where we allow each client to maintain a personalized, architecturally heterogeneous model during P2P cross-client training.

2) *Evaluation Strategies:* We use the area under the ROC curve (AUC) as the primary evaluation metric to assess classification performance, as AUC provides a more robust measure

across varying thresholds and offers greater interpretability.

Given the limited sample sizes of the ABIDE and DERM7pt datasets, we adopt 5-fold cross-validation to report the final results. Specifically, for local performance, we report the average AUC across five folds for each client. For global performance, we first compute the average AUC across all centers within each fold, then report the mean and standard deviation across the five folds. Thus, we present both the local performance of each client and the overall global performance.

Additionally, we define two evaluation settings: Local Test and Global Test. In the Local Test, each client’s model is evaluated solely on its own local test dataset to assess its specialization capability. In the Global Test, each client’s model is evaluated on the test datasets of all clients, and the final performance is obtained by averaging the results across all clients, thereby assessing the model’s generalization ability. Please note that when computing the final performance in the Global Test, all clients’ test datasets are assigned equal weighting, regardless of their sample sizes, to mitigate potential arising from imbalanced data distributions across clients. Furthermore, it is worth noting that for several model-homogeneous methods—namely Centralized, FedAvg, FedProx, and FedCross—only a single shared model is maintained. Consequently, in the Global Test scenario, these methods yield only a mean performance result derived from 5-fold cross-validation, rather than individual global results for each client-specific model.

3) *Implementation Details:* All methods were trained to converge using a batch size of 8. For the ASD classification task, we configured the training process with 40 communication rounds, while for the skin lesion classification task, we used 45 communication rounds. Each round consisted of 5 training iterations. Notably, in P2P training scenarios, the number of training iterations per round was scaled to  $5 \times N$ , where  $N$  denotes the number of clients, to account for the distributed nature of the learning process.

In the ASD classification task, the spatial dimensions of the four 3D temporal statistics were downsampled to  $48 \times 48 \times 48$  and subsequently concatenated along the channel dimension to construct the input representation. For the skin lesion classification task, we exclusively employed dermoscopic images, which were resized to a uniform resolution of  $224 \times 224$  pixels to ensure consistency across the dataset.

To enhance generalization and robustness, we applied standard spatial data augmentation techniques, e.g. random flipping, rotation, translation, and scaling, to both the 3D fMRI statistics and the 2D dermoscopy images. Optimization was performed using the Adam optimizer with a learning rate of  $1 \times 10^{-4}$ , aimed at minimizing the joint mutual learning loss as formulated in Equation 2. Additionally, the balancing hyperparameter  $\gamma$  was empirically set to 1 for the ASD classification task and 100 for the skin lesion classification task.

### C. Experimental Results

1) *Performance Comparison with Baselines:* Table II and Table III present a comprehensive evaluation of our proposed FedSKD against state-of-the-art baselines in both model-

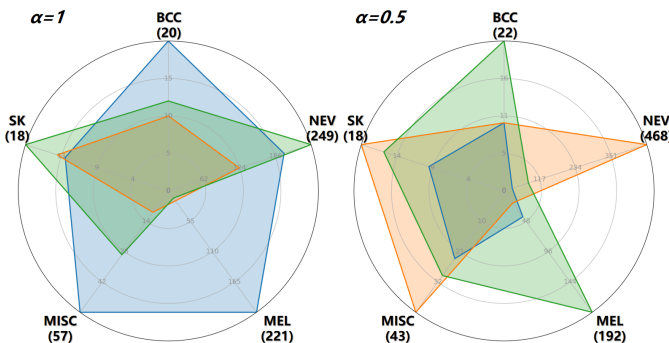


Fig. 4. Distribution of non-IID data across the clients in our FedSkin datasets for skin lesion classification. Different colors represent different clients with unique non-IID distributions.

TABLE II

PERFORMANCE COMPARISON ACROSS METHODS IN THE LOCAL AND GLOBAL TEST SCENARIOS ON THE FEDASD DATASET. THE BEST RESULTS UNDER THE MODEL-HETEROGENEOUS SETTING ARE HIGHLIGHTED IN BOLD. THE SYMBOL \* INDICATES THAT THE PERFORMANCE DIFFERENCE BETWEEN OUR FEDSKD AND THE SECOND-BEST BASELINE METHODS UNDER THE SAME FL SETTING IS STATISTICALLY SIGNIFICANT AT  $p < 0.05$ .

Method (FedASD)	Local Test					Global Test				
	$M_{Europe}$	$M_{WestUS}$	$M_{CentralUS}$	$M_{EastUS}$	Mean	$M_{Europe}$	$M_{WestUS}$	$M_{CentralUS}$	$M_{EastUS}$	Mean
<b>Homogeneous Models</b>										
Centralized	70.27±5.40	71.02±6.14	75.55±5.43	72.92±5.40	72.44±2.27	59.53±4.00	62.60±2.78	62.10±2.85	60.47±2.74	67.65±2.30
Local	66.40±6.48	68.06±3.93	66.41±4.15	70.23±4.64	67.77±2.69	59.53±4.00	62.60±2.78	62.10±2.85	60.47±2.74	61.17±2.05
FedAvg	69.21±6.21	73.18±2.05	67.94±6.61	69.36±4.86	69.92±2.55					64.70±1.79
FedProx	65.62±5.31	70.36±4.13	67.06±4.67	69.01±5.08	68.01±1.61					64.55±3.16
FedBN	69.48±4.83	68.69±3.53	72.47±3.89	69.52±8.01	70.04±2.88	65.48±1.99	66.15±1.94	65.57±2.55	64.31±2.97	65.38±2.18
FedCross	72.75±5.01	72.23±6.96	78.00±3.77	69.92±5.87	73.23±2.70					66.12±2.97
FedSKD	79.80±7.63	76.30±7.16	81.20±3.19	73.93±4.66	77.81±1.72	66.49±2.66	67.83±3.24	68.18±3.10	67.70±3.02	67.55±2.75
<b>Heterogeneous Models</b>										
Centralized	66.76±7.35	72.87±3.91	75.05±2.19	69.18±6.44	70.97±2.12	65.85±2.54	67.13±1.90	65.18±1.68	65.91±2.20	66.02±1.79
Local	68.90±2.13	67.06±4.16	69.74±5.30	69.03±4.07	68.69±2.73	60.34±1.68	61.01±2.85	61.78±1.07	61.08±1.56	61.05±1.23
FedCross <sup>†</sup>	70.67±3.11	70.13±5.69	72.67±3.25	71.60±5.78	71.27±3.17	63.33±4.33	62.89±5.16	63.90±2.68	63.51±3.54	63.41±3.57
FedSKD	75.83±4.22	76.14±4.30	79.83±6.68	74.86±4.45	<b>76.66±2.70*</b>	67.44±2.13	66.36±2.29	67.93±3.02	66.69±3.47	<b>67.10±2.23*</b>

TABLE III

PERFORMANCE COMPARISON ACROSS METHODS IN THE LOCAL AND GLOBAL TEST SCENARIOS ON THE FEDSKIN DATASETS. THE BEST RESULTS UNDER THE MODEL-HETEROGENEOUS SETTING ARE HIGHLIGHTED IN BOLD. THE SYMBOL \* INDICATES THAT THE PERFORMANCE DIFFERENCE BETWEEN OUR FEDSKD AND THE SECOND-BEST BASELINE METHODS UNDER THE SAME FL SETTING IS STATISTICALLY SIGNIFICANT AT  $p < 0.02$ .

Method FedSkin ( $\alpha=1$ )	Local Test				Global Test			
	$M_1$	$M_2$	$M_3$	Mean	$M_1$	$M_2$	$M_3$	Mean
<b>Homogeneous Models</b>								
Centralized	86.41±3.31	85.67±4.63	85.40±5.61	85.83±1.68	79.61±3.44	75.84±2.32	72.13±3.66	82.43±1.91
Local	81.06±6.48	81.97±9.21	76.76±7.04	79.93±4.18	79.61±3.44	75.84±2.32	72.13±3.66	75.86±2.47
FedAvg	84.52±2.73	82.30±7.47	84.97±6.06	83.93±3.39				81.67±3.44
FedProx	82.97±3.91	79.83±6.91	83.86±4.81	82.22±3.63				79.63±4.13
FedBN	81.47±6.55	78.68±4.66	81.42±5.15	80.52±2.66	78.60±3.57	75.83±5.29	76.29±3.82	76.91±3.52
FedCross	83.56±4.65	88.41±4.73	84.56±6.57	85.51±3.66				81.66±2.56
FedSKD	87.28±3.70	91.36±4.67	86.82±5.90	88.49±1.35	84.35±0.84	84.33±1.83	85.10±0.70	84.59±0.87
<b>Heterogeneous Models</b>								
Centralized	86.37±3.82	86.15±5.28	86.18±5.40	86.23±1.94	83.32±1.31	82.61±1.75	83.79±2.53	83.24±1.36
Local	81.35±3.90	81.95±7.75	78.77±7.63	80.69±3.91	78.47±3.70	75.44±2.27	73.21±2.73	75.70±2.05
FedCross <sup>†</sup>	82.47±3.04	88.18±4.71	85.41±4.98	85.69±1.64	81.11±1.59	81.19±1.13	81.33±1.31	81.21±1.02
FedSKD	88.41±3.04	90.50±3.50	87.59±4.89	<b>88.83±1.85*</b>	84.56±1.69	84.58±2.42	83.65±2.66	<b>84.26±2.13*</b>
<b>Homogeneous Models</b>								
Centralized	86.40±3.25	82.42±3.47	86.14±4.73	84.99±2.36	75.25±2.85	70.54±1.15	78.25±2.14	82.23±2.49
Local	80.93±4.67	75.38±5.20	78.84±2.96	78.38±1.98	75.25±2.85	70.54±1.15	78.25±2.14	74.68±1.48
FedAvg	82.03±4.80	79.87±2.05	81.46±3.14	81.12±1.42				78.82±2.18
FedProx	83.08±4.22	78.23±6.22	78.48±2.66	79.93±1.99				77.46±2.05
FedBN	79.06±6.27	78.23±3.99	76.01±3.33	77.77±2.49	75.35±3.59	75.99±3.51	75.31±3.70	75.55±3.23
FedCross	87.30±3.76	79.84±4.67	81.62±2.85	82.92±2.87				79.49±3.54
FedSKD	89.15±3.62	86.65±4.64	86.29±3.09	87.36±2.79	83.70±1.67	83.10±2.20	83.75±1.89	83.52±1.80
<b>Heterogeneous Models</b>								
Centralized	88.14±1.74	82.21±5.77	85.74±4.39	85.37±2.23	82.68±2.30	82.16±3.39	80.93±2.49	81.93±2.54
Local	79.95±4.23	72.45±6.05	80.06±2.23	77.49±3.13	73.99±3.49	71.36±3.01	76.73±2.64	74.03±1.32
FedCross <sup>†</sup>	86.14±2.77	82.83±2.03	82.78±3.00	83.92±2.07	80.32±1.71	80.01±3.28	79.73±1.34	80.02±1.74
FedSKD	89.27±2.94	85.40±2.80	87.37±1.25	<b>87.35±1.52*</b>	84.27±1.78	82.61±2.18	84.05±1.87	<b>83.64±1.81*</b>

homogeneous and model-heterogeneous settings. The evaluation is conducted under Local Test and Global Test scenarios for our two tasks.

As shown in Table II, in model-heterogeneous setting, FedSKD achieves state-of-the-art global average performance for ASD Classification across both test settings, with mean AUC values of 76.66% (Local Test) and 67.10% (Global Test), outperforming FedCross<sup>†</sup>, the leading heterogeneous P2P FL baseline, by significant margins of 5.39% and 3.44%, respectively. Notably, FedSKD also surpasses our lower-bound baseline (Local) by substantial margins of 7.97% and

6.05%, demonstrating its robust adaptation to heterogeneous data distributions. Similar superiority is observed in model-homogeneous settings, where FedSKD exceeds homogeneous FedCross by 5.39% and 3.44% while also significantly outperforming all homogeneous baselines.

The quantitative results summarized in Table III further highlight the superiority of FedSKD in Skin Lesion Classification under varying non-IID data distributions ( $\alpha=1$  and  $\alpha=0.5$ ). Notably, in model-heterogeneous setting, FedSKD consistently achieves the highest mean AUC values in both test scenarios, outperforming FedCross<sup>†</sup> by 3.14% and 3.05%



( $\alpha=1$ ) and by 3.43% and 3.62% ( $\alpha=0.5$ ) for Local and Global Tests, respectively. The performance gaps widen further when compared to the Local baseline, with improvements of 8.14% and 8.56% ( $\alpha=1$ ) and 9.86% and 9.61% ( $\alpha=0.5$ ). Under the homogeneous configurations, FedSKD maintains substantial leads over FedCross (2.98% and 2.93% ( $\alpha=1$ ) and by 4.44% and 4.03% ( $\alpha=0.5$ )) and other baselines.

Three critical insights emerge from these findings: First, aggregation-free P2P methods (FedSKD, FedCross variants) consistently outperform aggregation-based approaches (FedAvg, FedProx, FedBN) across all settings, highlighting the inherent limitations of parameter averaging in handling data heterogeneity. Second, FedSKD consistently outperforms FedCross in both homogeneous and heterogeneous settings, validating that our similarity knowledge distillation (SKD) mechanism effectively mitigates model drift and knowledge dilution through bidirectional feature-space regularization (i.e. multi-dimensional SKD). Third, the simultaneous improvement in Local Test (personalization) and Global Test (generalization) metrics demonstrates FedSKD’s unique capability to balance client-specific adaptation with cross-client knowledge fusion.

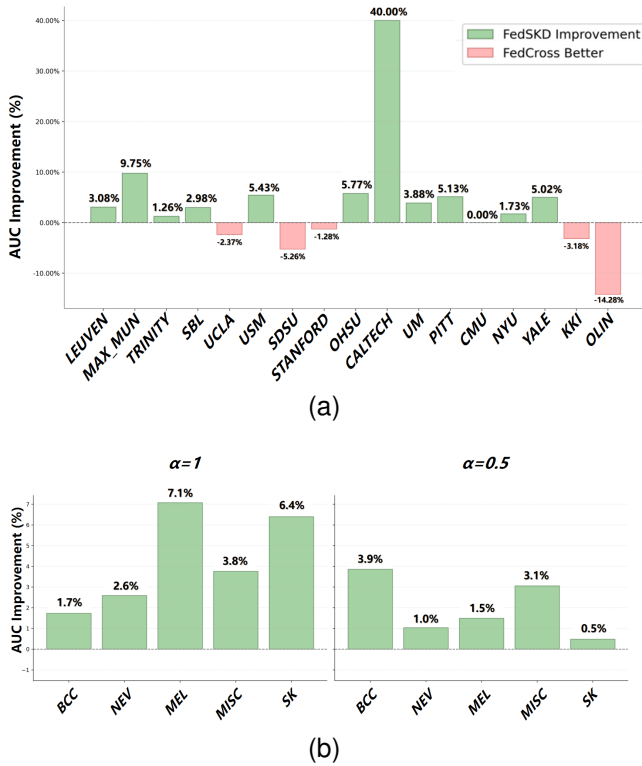


Fig. 5. Comparison of AUC Improvements: FedSKD vs. FedCross. (a) Summary of AUC performance gain across 17 institutions from the FedASD dataset (Table I), comparing FedSKD and FedCross. (b) Summary of AUC performance gain across 5 skin lesion types from the FedSkin dataset (Figure 4), comparing FedSKD and FedCross.

Consolidated predictions from all client models under 5-fold cross-validation reveal FedSKD’s consistent superiority. For ASD classification across 17 institutions in the ABIDE dataset (Figure 5 (a)), FedSKD achieves higher accuracy in the majority of institutions compared to FedCross. In skin lesion diagnosis (Figure 5 (b)), FedSKD demonstrates uniform improvements across all five lesion types under both Non-IID

settings ( $\alpha=1$  and  $\alpha=0.5$ ), with particularly significant gains in rare lesion categories (e.g. BCC and SK), underscoring its effectiveness in handling class imbalance.

These results collectively establish FedSKD as a paradigm-shifting framework that addresses fundamental limitations in both traditional P2P (such as model drift and knowledge dilution) and aggregation-based FL approaches (which suffer from performance degradation).

2) **Ablation Studies: Component-wise Analysis of SKD Effectiveness:** Table IV validates the contribution of each similarity dimension in our multi-dimensional SKD through model-heterogeneous ablation experiments. The results demonstrate that the complete SKD implementation, which integrates all similarity learning, achieves optimal performance across both tasks, highlighting the complementary nature of multi-granularity feature alignment. Notably, batch-wise SKD provides the most significant performance boost compared to pixel/voxel-wise components, as inter-sample correlations prove more discriminative than fine-grained spatial correspondences for image-level classification tasks. Furthermore, even variants with partial SKD configurations consistently outperform FedCross (in Table II-III), particularly in Local Test scenarios, underscoring the robustness of our method against knowledge fragmentation in peer-to-peer FL. The progressive performance improvement from single-to-full SKD configurations demonstrates FedSKD’s ability to synergistically address model drift through hierarchical feature alignment.

TABLE IV  
ABLATION STUDY ON DISTILLATION TYPES IN MULTI-DIMENSIONAL SKD. (A) RESULTS ON THE FEDASD DATASET. (B) RESULTS ON THE FEDSKIN DATASETS.

Similarity		Local Test (%)		Global Test (%)	
Batch	Voxel	Mean	Std	Mean	Std
✓		74.61	1.69	65.115	3.12
	✓	73.85	3.32	65.53	2.92
		74.71	2.40	66.97	2.27
✓	✓	75.34	2.65	66.31	2.53
✓		75.45	1.92	67.00	2.50
✓	✓	76.66	2.70	67.10	2.23

(a)

Similarity		Local Test (%)		Global Test (%)	
Batch	Pixel	Mean	Std	Mean	Std
$\alpha=1$					
✓		87.86	1.97	84.01	1.49
	✓	87.29	2.04	82.62	1.61
✓	✓	88.83	1.85	84.26	2.13
$\alpha=0.5$					
✓		86.06	1.50	82.60	1.36
	✓	84.95	2.20	81.52	2.29
✓	✓	87.35	1.52	83.64	1.81

(b)

**Layer-wise Analysis of SKD Effectiveness:** To investigate how hierarchical feature distillation impacts the DAM-KTM mutual learning within our FedSKD framework, we conduct a layer-wise ablation study under model-heterogeneous setting.

Building on the established principle that deep networks progressively encode features from low-level textures to high-level semantics [53], we hypothesize that deeper layers capture more task-aligned semantic representations. Therefore, our experimental design initiates from the deepest layer (Layer 4 of ResNet-10), where feature embeddings exhibit the strongest correlation with classification objectives, and incrementally incorporates shallower layers (Layer 3  $\rightarrow$  Layer 2  $\rightarrow$  Layer 1) to systematically evaluate multi-scale feature alignment.

TABLE V

ABLATION STUDY ON ACTIVATED LAYERS IN SIMILARITY KNOWLEDGE DISTILLATION. (A) RESULTS ON THE FEDASD DATASET. (B) RESULTS ON THE FEDSKIN DATASETS.

Layer				Local Test (%)		Global Test (%)	
1	2	3	4	Mean	Std	Mean	Std
			✓	75.58	2.60	66.75	2.45
		✓	✓	74.31	2.89	65.95	3.60
	✓	✓	✓	75.90	1.36	65.73	1.96
✓	✓	✓	✓	76.66	2.70	67.10	2.23

(a)

Layer				Local Test (%)		Global Test (%)	
1	2	3	4	Mean	Std	Mean	Std
$\alpha=1$							
			✓	88.66	1.11	84.01	1.26
		✓	✓	88.60	2.24	84.68	1.37
	✓	✓	✓	88.68	2.06	84.25	1.88
✓	✓	✓	✓	88.83	1.85	84.26	2.13
$\alpha=0.5$							
			✓	87.12	1.53	83.32	1.86
		✓	✓	86.86	1.96	83.41	1.49
	✓	✓	✓	87.11	2.08	83.87	2.08
✓	✓	✓	✓	87.35	1.52	83.64	1.81

(b)

As shown in Table V, performance metrics for both ASD and skin lesion classification improve progressively as SKD engages broader network depths. The full configuration—utilizing all four ResNet-10 layers—achieves peak performance, demonstrating that knowledge transfer across clients is significantly enhanced when multi-level feature representations participate in the distillation process. Specifically, while deep layers encode task-specific semantics critical for diagnostic decision-making, shallow layers preserve spatial and textural biomarkers essential for robust generalization. This hierarchical synergy underscores the importance of multi-level feature alignment in federated learning, where both localized and global representations contribute to mitigating model drift and improving cross-client knowledge fusion.

**Timing for Multi-dimensional SKD Integration:** To determine the optimal timing for introducing our multi-dimensional SKD into the FedSKD framework, we conduct a study varying the timing to activate multi-dimensional SKD, including 0% (training onset), 25%, 50%, and 75% of total communication rounds. Please note here that prior to SKD activation, models follow standard P2P transfer with target client adaptation. As Table VI demonstrates, a strong temporal dependency emerges: earlier SKD integration yields progressively greater performance gains, with introducing SKD at training on-

set achieves peak performance across both tasks and across both evaluation settings. By constraining parameter divergence through early feature-space (i.e. multi-dimensional SKD) regularization, FedSKD prevents irreversible model drift while preserving client-specific knowledge. The performance degradation observed with delayed SKD activation underscores the importance of proactive knowledge preservation in P2P FL systems.

TABLE VI

ABLATION STUDY ON ACTIVATED TIMING FOR SIMILARITY KNOWLEDGE DISTILLATION. (A) RESULTS ON THE FEDASD DATASET. (B) RESULTS ON THE FEDSKIN DATASETS.

KD Round (%)	Local Test (%)		Global Test (%)	
	Mean	Std	Mean	Std
0	76.66	2.70	67.10	2.23
25	75.33	2.27	66.99	2.46
50	73.75	1.65	65.66	2.12
75	73.19	2.81	65.79	2.95

(a)

KD Round (%)	Local Test (%)		Global Test (%)	
	Mean	Std	Mean	Std
$\alpha=1$				
0	88.83	1.85	84.26	2.13
25	88.20	1.09	84.62	1.26
50	87.65	1.99	84.10	1.08
75	87.37	2.28	83.81	1.95
$\alpha=0.5$				
0	87.35	1.52	83.64	1.81
25	86.28	1.61	83.25	1.57
50	86.12	2.32	83.17	2.06
75	85.23	2.05	82.24	2.68

(b)

**Impact on Fairness Improvement:** We further investigate the effect of FedSDK on improving fairness, and we focus on outcome-consistency group fairness [54]–[57] with respect to the sex attribute (male vs. female) here. For this analysis, we consider only the local test setting, where each client’s model is evaluated exclusively on its own dataset to measure fairness. We employ the maximum AUC gap ( $\Delta_{auc}$ ) as our fairness metric, defined as the difference between the highest and lowest AUC values across sex subgroups in Equation 16, to measure disparities in model performance:

$$\Delta_{auc} = \left| \frac{1}{N} \sum_{k=1}^N AUC_{male}^k - \frac{1}{N} \sum_{k=1}^N AUC_{female}^k \right| \quad (16)$$

where  $AUC_{male}^k$  and  $AUC_{female}^k$  represent the AUC values for male and female subgroups, respectively, computed on the dataset  $D_k$  of the  $k$ -th client;  $N$  is the total number of clients; and  $|\cdot|$  denotes the absolute value operation. We compare the sex fairness of our FedSKD with FedCross, on both classification tasks. As we can see from Table VII, the results demonstrate that our method not only improves the average AUC but also significantly reduces the disparity between them. For instance, in the ASD classification task, our approach achieves a 6.37% improvement in fairness, effectively mitigating unfairness related to the sensitive attribute.

TABLE VII  
COMPARISON OF FAIRNESS PERFORMANCE OF FEDCROSS AND FEDSKD ON SEX ATTRIBUTE ON BOTH FEDASD DATASET (LEFT) AND FEDSKIN DATASET (RIGHT).

Method	FedASD				FedSkin							
	Male $\uparrow$	Female $\uparrow$	Avg $\uparrow$	$\Delta\downarrow$	$\alpha=1$				$\alpha=0.5$			
					Male $\uparrow$	Female $\uparrow$	Avg $\uparrow$	$\Delta\downarrow$	Male $\uparrow$	Female $\uparrow$	Avg $\uparrow$	$\Delta\downarrow$
FedCross	67.46	79.60	73.53	12.14	86.77	81.59	84.18	5.18	88.88	81.34	85.11	7.54
FedSKD	71.57	77.34	<b>74.46</b>	<b>5.77</b>	89.79	85.26	<b>87.52</b>	<b>4.54</b>	88.27	86.08	<b>87.17</b>	<b>2.19</b>

#### IV. DISCUSSION

Our proposed FedSKD framework addresses two critical challenges in federated learning: model heterogeneity, enabled by its aggregation-free peer-to-peer (P2P) architecture, and model drift and knowledge dilution, mitigated through hierarchical similarity knowledge distillation (SKD). *First*, FedSKD eliminates reliance on centralized aggregation, a major limitation of existing aggregation-dependent MHFL methods that imposes substantial server-side computational and storage overhead. As detailed in Section 2, our framework operates entirely without server-side aggregation, model maintenance, or additional computation, instead enabling direct model exchanges between clients. This paradigm not only reduces infrastructure demands but also circumvents performance degradation caused by gradient conflicts in weight aggregation, as evidenced by the superior performance of aggregation-free baselines (FedCross<sup>†</sup> and FedCross) over classical aggregation-dependent methods (FedAvg, FedProx, FedBN) in Table II and Table III. Furthermore, its model-agnostic design makes it applicable to both heterogeneous and homogeneous FL settings, positioning it as a scalable and versatile solution for real-world deployments.

*Second*, FedSKD introduces a multi-dimensional similarity knowledge distillation mechanism to facilitate semantically rich, bidirectional knowledge transfer between clients. By integrating batch-wise, pixel/voxel-wise, and region-wise SKD within a mutual learning paradigm, FedSKD enables clients to extract task-specific features that generalize across non-IID data distributions. Specifically, multi-dimensional SKD preserves local specificity by aligning fine-grained spatial patterns (via pixel/voxel-level distillation), maintains global consistency through batch-level semantic correlation matching, and anchors clinically critical interdependencies via region-wise functional connectivity distillation. During training, clients distill their local expertise into received KTM while constraining updates via frozen prediction heads, preventing catastrophic forgetting of cross-client knowledge. Simultaneously, DAMs assimilate cross-institutional insights from KTM through multi-level feature alignment, ensuring progressive adaptation without divergence. This bidirectional exchange mitigates model drift by enforcing continuous feature-space alignment and counters knowledge dilution by reinforcing critical diagnostic patterns. As shown in Table II, Table III, and Table IV, FedSKD variants incorporating partial SKD consistently outperform FedCross across all configurations, with the full SKD ensemble achieving the highest AUC. Further validation in Figure 5 highlights FedSKD’s superior performance over FedCross<sup>†</sup> across 17 institutions in the ABIDE dataset, as well

as its strong generalization on Derm7pt, which we attribute to SKD’s anti-dilution properties.

Additionally, as demonstrated in both Local and Global Test scenarios, FedSKD enhances personalization (client-specific accuracy) while improving generalization (cross-institutional adaptability). Notably, Table III and Table IV indicate that FedSKD surpasses the idealized “Centralized” baseline, where clients have access to all data. This achievement is particularly striking given the pronounced non-IID characteristics of medical imaging data, where variations in acquisition protocols, scanner types, and patient demographics inherently degrade model performance. Thus, FedSKD’s ability to reliably mitigate data distribution shifts while accommodating model heterogeneity underscores its robustness in clinically realistic FL scenarios.

While FedSKD represents a significant advancement in model-heterogeneous federated learning, several limitations warrant further exploration. *First*, this study evaluated FedSKD primarily in the context of medical image classification. Although the framework can theoretically extend to other medical imaging tasks, such as segmentation and detection, adapting the task model structure (e.g., from a classification to a segmentation model) requires further validation. Future work will explore FedSKD’s performance across a broader range of medical imaging applications. *Second*, the mutual learning process necessitates the simultaneous training of both DAM and KTM per client, effectively doubling computational costs compared to single-model frameworks. While modern GPU hardware mitigates concerns regarding model size, reducing computational overhead remains crucial. Future research will investigate iterative training paradigms to decouple DAM-KTM updates and explore lightweight distillation techniques, such as attention-based or feature map distillation [58], [59], to enhance efficiency without sacrificing performance. *Third*, the aggregation-free paradigm requires clients to exchange entire models during peer-to-peer transfers, posing potential risks of data leakage through model inversion attacks, membership inference, or gradient extraction [60]. To address these privacy concerns, client-side encryption techniques, such as partially homomorphic encryption (e.g., Paillier encryption) [61], could enable secure model sharing without exposing raw parameters. *Lastly*, FedSKD operates in a fully aggregation-free setting, but hybrid approaches that integrate lightweight server-side aggregation (e.g., feature fusion for critical knowledge) with client-side model transfer could offer additional benefits. Future work will explore hybrid frameworks where selective aggregation at trusted nodes complements peer-to-peer SKD, potentially enhancing both performance and privacy

preservation.

## V. CONCLUSION

In this paper, we propose FedSKD, a peer-to-peer federated learning framework that addresses model heterogeneity by enabling direct knowledge exchange via round-robin circulation of heterogeneous client models. This approach eliminates server dependency while mitigating performance degradation associated with traditional aggregation-dependent methods. Central to FedSKD is our multi-dimensional similarity knowledge distillation (batch-, pixel/voxel-, and region-wise), which ensures bidirectional, semantically rich knowledge transfer across clients. This mechanism prevents catastrophic knowledge forgetting and model drift through progressive refinement and distribution alignment. Extensive evaluations on FedASD (ASD classification) and FedSkin (skin lesion diagnosis) demonstrate FedSKD's superior generalization and personalization capabilities, validating its applicability to real-world medical FL scenarios.

## ACKNOWLEDGMENTS

This research was supported by Australian Government Research Training Program (RTP) scholarship.

## REFERENCES

- [1] X. Li, Y. Gu, N. Dvornek, L. H. Staib, P. Ventola, and J. S. Duncan, "Multi-site fmri analysis using privacy-preserving federated learning and domain adaptation: Abide results," *Medical image analysis*, vol. 65, p. 101765, 2020.
- [2] H. Guan, P.-T. Yap, A. Bozoki, and M. Liu, "Federated learning for medical image analysis: A survey," *Pattern Recognition*, p. 110424, 2024.
- [3] C. G. Kels, "Hipa in the era of data sharing," *JAMA*, vol. 323, no. 5, pp. 476–477, 2020.
- [4] P. Voigt and A. Von dem Bussche, "The eu general data protection regulation (gdpr)," *A Practical Guide, 1st Ed., Cham: Springer International Publishing*, vol. 10, no. 3152676, pp. 10–5555, 2017.
- [5] M. Parasol, "The impact of china's 2016 cyber security law on foreign technology firms, and on china's big data and smart city dreams," *Computer law & security review*, vol. 34, no. 1, pp. 67–98, 2018.
- [6] L. Peng, N. Wang, N. Dvornek, X. Zhu, and X. Li, "Fedni: Federated graph learning with network inpainting for population-based disease prediction," *IEEE Transactions on Medical Imaging*, vol. 42, no. 7, pp. 2032–2043, 2022.
- [7] Z. Fan, J. Su, K. Gao, D. Hu, and L.-L. Zeng, "A federated deep learning framework for 3d brain mri images," in *2021 international joint conference on neural networks (IJCNN)*. IEEE, 2021, pp. 1–6.
- [8] B. McMahan, E. Moore, D. Ramage, S. Hampson, and B. A. y Arcas, "Communication-efficient learning for deep networks from decentralized data," in *Artificial intelligence and statistics*. PMLR, 2017, pp. 1273–1282.
- [9] R. Yan, L. Qu, Q. Wei, S.-C. Huang, L. Shen, D. L. Rubin, L. Xing, and Y. Zhou, "Label-efficient self-supervised federated learning for tackling data heterogeneity in medical imaging," *IEEE Transactions on Medical Imaging*, vol. 42, no. 7, pp. 1932–1943, 2023.
- [10] J. Wicaksana, Z. Yan, X. Yang, Y. Liu, L. Fan, and K.-T. Cheng, "Customized federated learning for multi-source decentralized medical image classification," *IEEE Journal of Biomedical and Health Informatics*, vol. 26, no. 11, pp. 5596–5607, 2022.
- [11] M. Yashwanth, G. K. Nayak, A. Singh, Y. Simmhan, and A. Chakraborty, "Adaptive self-distillation for minimizing client drift in heterogeneous federated learning," *arXiv preprint arXiv:2305.19600*, 2023.
- [12] T. Li, A. K. Sahu, M. Zaheer, M. Sanjabi, A. Talwalkar, and V. Smith, "Federated optimization in heterogeneous networks," *Proceedings of Machine learning and systems*, vol. 2, pp. 429–450, 2020.
- [13] X. Li, M. Jiang, X. Zhang, M. Kamp, and Q. Dou, "Fedbn: Federated learning on non-iid features via local batch normalization," *arXiv preprint arXiv:2102.07623*, 2021.
- [14] N. K. Dinsdale, M. Jenkinson, and A. I. Namburete, "Fedharmony: Unlearning scanner bias with distributed data," in *International Conference on Medical Image Computing and Computer-Assisted Intervention*. Springer, 2022, pp. 695–704.
- [15] P. Guo, P. Wang, J. Zhou, S. Jiang, and V. M. Patel, "Multi-institutional collaborations for improving deep learning-based magnetic resonance image reconstruction using federated learning," in *Proceedings of the IEEE/CVF conference on computer vision and pattern recognition*, 2021, pp. 2423–2432.
- [16] X. He, C. Tan, B. Liu, L. Si, W. Yao, L. Zhao, D. Liu, Q. Zhangli, Q. Chang, K. Li *et al.*, "Dealing with heterogeneous 3d mr knee images: A federated few-shot learning method with dual knowledge distillation," in *2023 IEEE 20th International Symposium on Biomedical Imaging (ISBI)*. IEEE, 2023, pp. 1–5.
- [17] Z. Zhu, J. Hong, and J. Zhou, "Data-free knowledge distillation for heterogeneous federated learning," in *International conference on machine learning*. PMLR, 2021, pp. 12 878–12 889.
- [18] X. Gong, A. Sharma, S. Karanam, Z. Wu, T. Chen, D. Doermann, and A. Innanje, "Ensemble attention distillation for privacy-preserving federated learning," in *Proceedings of the IEEE/CVF International Conference on Computer Vision*, 2021, pp. 15 076–15 086.
- [19] M. Tom Yeh *et al.*, "Designing a moral compass for the future of computer vision using speculative analysis," in *Proceedings of the IEEE Conference on Computer Vision and Pattern Recognition Workshops*, 2017, pp. 64–73.
- [20] N. Rieke, J. Hancox, W. Li, F. Milletari, H. R. Roth, S. Albarqouni, S. Bakas, M. N. Galtier, B. A. Landman, K. Maier-Hein *et al.*, "The future of digital health with federated learning," *NPJ digital medicine*, vol. 3, no. 1, pp. 1–7, 2020.
- [21] F. Zhang, H. Liu, Q. Cai, C.-M. Feng, B. Wang, S. Wang, J. Dong, and D. Zhang, "Federated cross-incremental self-supervised learning for medical image segmentation," *IEEE Transactions on Neural Networks and Learning Systems*, pp. 1–14, 2024.
- [22] P. Kairouz, H. B. McMahan, B. Avent, A. Bellet, M. Bennis, A. N. Bhagoji, K. Bonawitz, Z. Charles, G. Cormode, R. Cummings *et al.*, "Advances and open problems in federated learning," *Foundations and trends® in machine learning*, vol. 14, no. 1–2, pp. 1–210, 2021.
- [23] Y. Shi, Y. Zhou, and Y. Shi, "Over-the-air decentralized federated learning," in *2021 IEEE International Symposium on Information Theory (ISIT)*. IEEE, 2021, pp. 455–460.
- [24] S. Chen, D. Yu, Y. Zou, J. Yu, and X. Cheng, "Decentralized wireless federated learning with differential privacy," *IEEE Transactions on Industrial Informatics*, vol. 18, no. 9, pp. 6273–6282, 2022.
- [25] A. G. Roy, S. Siddiqui, S. Pölsterl, N. Navab, and C. Wachinger, "Braintorrent: A peer-to-peer environment for decentralized federated learning," *arXiv preprint arXiv:1905.06731*, 2019.
- [26] L. Yuan, Y. Ma, L. Su, and Z. Wang, "Peer-to-peer federated continual learning for naturalistic driving action recognition," in *Proceedings of the IEEE/CVF Conference on Computer Vision and Pattern Recognition*, 2023, pp. 5250–5259.
- [27] X. Xu, H. H. Deng, T. Chen, T. Kuang, J. C. Barber, D. Kim, J. Gateno, J. J. Xia, and P. Yan, "Federated cross learning for medical image segmentation," in *Medical Imaging with Deep Learning*. PMLR, 2024, pp. 1441–1452.
- [28] D. Li and J. Wang, "Fedmd: Heterogenous federated learning via model distillation," *arXiv preprint arXiv:1910.03581*, 2019.
- [29] A. Afonin and S. P. Karimireddy, "Towards model agnostic federated learning using knowledge distillation," *arXiv preprint arXiv:2110.15210*, 2021.
- [30] C.-Y. Huang, K. Srinivas, X. Zhang, and X. Li, "Overcoming data and model heterogeneities in decentralized federated learning via synthetic anchors," *arXiv preprint arXiv:2405.11525*, 2024.
- [31] H. Chang, V. Shejwalkar, R. Shokri, and A. Houmansadr, "Cronus: Robust and heterogeneous collaborative learning with black-box knowledge transfer," *arXiv preprint arXiv:1912.11279*, 2019.
- [32] T. Lin, L. Kong, S. U. Stich, and M. Jaggi, "Ensemble distillation for robust model fusion in federated learning," *Advances in neural information processing systems*, vol. 33, pp. 2351–2363, 2020.
- [33] S. Cheng, J. Wu, Y. Xiao, and Y. Liu, "Fedgems: Federated learning of larger server models via selective knowledge fusion," *arXiv preprint arXiv:2110.11027*, 2021.
- [34] S. Itahara, T. Nishio, Y. Koda, M. Morikura, and K. Yamamoto, "Distillation-based semi-supervised federated learning for communication-efficient collaborative training with non-iid private data," *IEEE Transactions on Mobile Computing*, vol. 22, no. 1, pp. 191–205, 2021.

- [35] Y. J. Cho, A. Manoel, G. Joshi, R. Sim, and D. Dimitriadis, "Heterogeneous ensemble knowledge transfer for training large models in federated learning," *arXiv preprint arXiv:2204.12703*, 2022.
- [36] J. Wang, X. Yang, S. Cui, L. Che, L. Lyu, D. D. Xu, and F. Ma, "Towards personalized federated learning via heterogeneous model reassembly," *Advances in Neural Information Processing Systems*, vol. 36, 2024.
- [37] C. Wu, F. Wu, L. Lyu, Y. Huang, and X. Xie, "Communication-efficient federated learning via knowledge distillation," *Nature communications*, vol. 13, no. 1, p. 2032, 2022.
- [38] L. Yi, H. Yu, Z. Shi, G. Wang, X. Liu, L. Cui, and X. Li, "Fedssa: Semantic similarity-based aggregation for efficient model-heterogeneous personalized federated learning," *arXiv preprint arXiv:2312.09006*, 2023.
- [39] Z. Qin, S. Deng, M. Zhao, and X. Yan, "Fedapen: personalized cross-silo federated learning with adaptability to statistical heterogeneity," in *Proceedings of the 29th ACM SIGKDD Conference on Knowledge Discovery and Data Mining*, 2023, pp. 1954–1964.
- [40] T. Shen, J. Zhang, X. Jia, F. Zhang, Z. Lv, K. Kuang, C. Wu, and F. Wu, "Federated mutual learning: a collaborative machine learning method for heterogeneous data, models, and objectives," *Frontiers of Information Technology & Electronic Engineering*, vol. 24, no. 10, pp. 1390–1402, 2023.
- [41] L. Yi, H. Yu, C. Ren, G. Wang, X. Liu, and X. Li, "Federated model heterogeneous matryoshka representation learning," *arXiv preprint arXiv:2406.00488*, 2024.
- [42] L. Yi, H. Yu, C. Ren, H. Zhang, G. Wang, X. Liu, and X. Li, "Fedmoe: Data-level personalization with mixture of experts for model-heterogeneous personalized federated learning," *arXiv preprint arXiv:2402.01350*, 2024.
- [43] —, "pfedafm: Adaptive feature mixture for batch-level personalization in heterogeneous federated learning," *arXiv preprint arXiv:2404.17847*, 2024.
- [44] K. J. Friston, "Functional and effective connectivity: a review," *Brain connectivity*, vol. 1, no. 1, pp. 13–36, 2011.
- [45] E. Bullmore and O. Sporns, "Complex brain networks: graph theoretical analysis of structural and functional systems," *Nature reviews neuroscience*, vol. 10, no. 3, pp. 186–198, 2009.
- [46] S. R. Sharma, X. Gonda, and F. I. Tarazi, "Autism spectrum disorder: classification, diagnosis and therapy," *Pharmacology & Therapeutics*, vol. 190, pp. 91–104, 2018.
- [47] A. Di Martino, C.-G. Yan, Q. Li, E. Denio, F. X. Castellanos, K. Alaerts, J. S. Anderson, M. Assaf, S. Y. Bookheimer, M. Dapretto *et al.*, "The autism brain imaging data exchange: towards a large-scale evaluation of the intrinsic brain architecture in autism," *Molecular Psychiatry*, vol. 19, no. 6, pp. 659–667, 2014.
- [48] Z. Weng, W. Cai, and B. Zhou, "Efficient 4d fmri asd classification using spatial-temporal-omics-based learning framework," in *2025 IEEE International Symposium on Biomedical Imaging (ISBI)*. IEEE, 2025, pp. 1–4.
- [49] C. Craddock, S. Sikka, B. Cheung, R. Khanuja, S. S. Ghosh, C. Yan, Q. Li, D. Lurie, J. Vogelstein, R. Burns *et al.*, "Towards automated analysis of connectomes: The configurable pipeline for the analysis of connectomes (c-pac)," *Front Neuroinform*, vol. 42, no. 10.3389, 2013.
- [50] J. Zhang, Q. Wang, X. Wang, L. Qiao, and M. Liu, "Preserving specificity in federated graph learning for fmri-based neurological disorder identification," *Neural Networks*, vol. 169, pp. 584–596, 2024.
- [51] J. Kawahara, S. Daneshvar, G. Argenziano, and G. Hamarneh, "Seven-point checklist and skin lesion classification using multitask multimodal neural nets," *IEEE Journal of Biomedical and Health Informatics*, vol. 23, no. 2, pp. 538–546, 2019.
- [52] T. Bdair, N. Navab, and S. Albarqouni, "Fedperl: Semi-supervised peer learning for skin lesion classification," in *Medical Image Computing and Computer Assisted Intervention – MICCAI 2021: 24th International Conference, Strasbourg, France, September 27–October 1, 2021, Proceedings, Part III*. Berlin, Heidelberg: Springer-Verlag, 2021, p. 336–346. [Online]. Available: [https://doi.org/10.1007/978-3-030-87199-4\\_32](https://doi.org/10.1007/978-3-030-87199-4_32)
- [53] M. D. Zeiler and R. Fergus, "Visualizing and understanding convolutional networks," in *Computer Vision—ECCV 2014: 13th European Conference, Zurich, Switzerland, September 6–12, 2014, Proceedings, Part I 13*. Springer, 2014, pp. 818–833.
- [54] Z. Xu, S. Zhao, Q. Quan, Q. Yao, and S. K. Zhou, "Fairadabn: Mitigating unfairness with adaptive batch normalization and its application to dermatological disease classification," in *International Conference on Medical Image Computing and Computer-Assisted Intervention*. Springer, 2023, pp. 307–317.
- [55] Z. Xu, F. Tang, Q. Quan, Q. Yao, and S. K. Zhou, "Apple: Adversarial privacy-aware perturbations on latent embedding for unfairness mitigation," *arXiv preprint arXiv:2403.05114*, 2024.
- [56] R. Jin, Z. Xu, Y. Zhong, Q. Yao, Q. Dou, S. K. Zhou, and X. Li, "Fairmedfm: fairness benchmarking for medical imaging foundation models," *arXiv preprint arXiv:2407.00983*, 2024.
- [57] Z. Xu, J. Li, Q. Yao, H. Li, M. Zhao, and S. K. Zhou, "Addressing fairness issues in deep learning-based medical image analysis: a systematic review," *npj Digital Medicine*, vol. 7, no. 1, p. 286, 2024.
- [58] S. Zagoruyko and N. Komodakis, "Paying more attention to attention: Improving the performance of convolutional neural networks via attention transfer," *arXiv preprint arXiv:1612.03928*, 2016.
- [59] J. Yim, D. Joo, J. Bae, and J. Kim, "A gift from knowledge distillation: Fast optimization, network minimization and transfer learning," in *Proceedings of the IEEE conference on computer vision and pattern recognition*, 2017, pp. 4133–4141.
- [60] L. Yuan, Z. Wang, L. Sun, S. Y. Philip, and C. G. Brinton, "Decentralized federated learning: A survey and perspective," *IEEE Internet of Things Journal*, 2024.
- [61] P. Paillier, "Public-key cryptosystems based on composite degree residuosity classes," in *International conference on the theory and applications of cryptographic techniques*. Springer, 1999, pp. 223–238.